Zhou *et al. Microstructures* 2022;2:2022018
**DOI:** 10.20517/microstructures.2022.13

**Microstructures**

**Research Article**

**Open Access**

Check for updates

# Tunable negative thermal expansion in $La(Fe, Si)_{13}$/resin composites with high mechanical property and long-term cycle stability

**He Zhou[1], Yuwei Liu[1], Rongjin Huang[2], Bo Chen[3], Min Xia[1], Ziyuan Yu[1], Haodong Chen[1], Kaiming Qiao[1], Junzhuang Cong[4], Sergey V. Taskaev[5], Ke Chu[6], Hu Zhang[1]**

[1]School of Materials Science and Engineering, University of Science and Technology Beijing, Beijing 100083, China.
[2]State Key Laboratory of Technologies in Space Cryogenic Propellants, Technical Institute of Physics and Chemistry, Chinese Academy of Sciences, Beijing 100049, China.
[3]Key Laboratory of Advanced Civil Engineering Materials (Ministry of Education), School of Materials Science and Engineering, Tongji University, Shanghai 201804, China.
[4]MultiFields Technologies (Beijing) Co. Ltd., Hengxing Building, Zhongguancun, Haidian Dist., Beijing 100190, China.
[5]Physics Faculty, Chelyabinsk State University, Chelyabinsk 454001, Russia.
[6]School of Materials Science and Engineering, Lanzhou Jiaotong University, Lanzhou 730070, Gansu, China.

**Correspondence to:** Prof. Hu Zhang, School of Materials Science and Engineering, University of Science and Technology Beijing, 30 Xueyuan Road, Haidian District, Beijing 100083, China. E-mail: zhanghu@ustb.edu.cn; Prof. Rongjin Huang, State Key Laboratory of Technologies in Space Cryogenic Propellants, Technical Institute of Physics and Chemistry, Chinese Academy of Sciences, 29 Zhongguancun East Road, Haidian District, Beijing 100049, China. E-mail: huangrongjin@mail.ipc.ac.cn; Dr. Bo Chen, Key Laboratory of Advanced Civil Engineering Materials (Ministry of Education), School of Materials Science and Engineering, Tongji University, 1239 Siping Road, Shanghai 201804, China. E-mail: bo.chen@tongji.edu.cn

**How to cite this article:** Zhou H, Liu Y, Huang R, Chen B, Xia M, Yu Z, Chen H, Qiao K, Cong J, Taskaev SV, Chu K, Zhang H. Tunable negative thermal expansion in $La(Fe, Si)_{13}$/resin composites with high mechanical property and long-term cycle stability. *Microstructures* 2022;2:2022018. https://dx.doi.org/10.20517/microstructures.2022.13

**Received:** 8 Jun 2022 **First Decision:** 14 Jul 2022 **Revised:** 4 Aug 2022 **Accepted:** 15 Aug 2022 **Published:** 17 Aug 2022

**Academic Editors:** Xiaozhou Liao, Yuzhu Song, Andrea Sanson **Copy Editor:** Fangling Lan **Production Editor:** Fangling Lan

## Abstract

Materials with tunable negative thermal expansion (NTE) are highly demanded in various functional devices. $La(Fe, Si)_{13}$-based compounds are promising NTE materials due to their outstanding NTE properties. However, their poor mechanical properties and related short service life restrict their practical applications. In this work, epoxy resin with positive thermal expansion is used to synthesize La-Fe-Si/resin composites. The NTE of La-Fe-Si/resin composites can be manipulated by optimizing the La-Fe-Si particle size and resin content, and tailoring resin content could tune the NTE more effectively. The average linear coefficient of thermal expansion of the composites decreases from -275.0 × $10^{-6}$ $K^{-1}$ to -4.9 × $10^{-6}$ $K^{-1}$ over the magnetic transition temperature range as the resin

content increases from 3 wt.% to 80 wt.%. In addition, zero thermal expansion is achieved in the La-Fe-Si/resin composite with 20 wt.% resin. The resin would reinforce the binding force by filling the pores between the particles. The La-Fe-Si/resin composite with 80 wt.% resin exhibits highly improved mechanical properties; for example, its compressive strength of 205 MPa is 75% higher than that of the La-Fe-Si/resin composite with 3 wt.% resin. The prepared La-Fe-Si/resin composites can be machined into different shapes for practical applications, such as thin plates, strips, and rods. Furthermore, the La-Fe-Si/resin composites can undergo 1000 thermal cycles without NTE performance degradation and mechanical integrity loss, indicating durable cycle stability. Hence, significantly tunable NTE with high mechanical properties and long-term cycle stability makes La-Fe-Si/resin composites present great application potential as NTE materials.

**Keywords:** Negative thermal expansion (NTE), La-Fe-Si compounds, mechanical properties

## INTRODUCTION

Most materials exhibit positive thermal expansion (PTE). However, various functional devices require precisely tailored thermal expansion or even zero thermal expansion (ZTE), such as high-precision optical mirrors, fiber reflective gratings, and printed circuit boards[1]. Therefore, materials with negative thermal expansion (NTE) have attracted increasing attention. This unusual volumetric effect can be used to regulate the coefficient of thermal expansion (CTE) and produce ZTE composites by mixing them with PTE materials. So far, a few kinds of materials have been reported as potential NTE material candidates, such as $ZrW_2O_8$[2], antiperovskite manganese nitrides[3], $AgB(CN)_4$[4], MM′X compounds[5], $\beta$-$Cu_{1.8}Zn_{0.2}V_2O_7$[6], (Hf, Nb)$Fe_2$[7], $ScF_3$-based compounds[8], and $PbTiO_3$-based compounds[9]. Nonetheless, most NTE materials cannot be used as thermal expansion compensators in practice because of their low NTE coefficient, limited NTE temperature window, and poor mechanical properties.

La(Fe, Si)$_{13}$-based compounds with a cubic $NaZn_{13}$-type structure (space group *Fm*3*c*) have been widely studied because of their giant magnetocaloric effect (MCE) and the application potential in magnetic refrigeration[10-12]. The large MCE of La(Fe, Si)$_{13}$-based compounds primarily originates from their itinerant electron metamagnetic (IEM) transition, that is, a field-induced first-order magnetic transition from the paramagnetic (PM) to ferromagnetic (FM) states[13]. Furthermore, La(Fe, Si)$_{13}$-based compounds have large magnetovolume effect (MVE); namely, the magnetic transition is accompanied by a distinct NTE behavior around the Curie temperature ($T_C$)[14]. Therefore, their isotropic and remarkable NTE suggests that La(Fe, Si)$_{13}$-based compounds could be excellent NTE materials for applications.

The NTE properties of La(Fe, Si)$_{13}$-based compounds have been reported in recent years. For example, the $LaFe_{10.5}Co_{1.0}Si_{1.5}$ compound exhibits a large NTE in a wide operation temperature window of 110 K, and its linear NTE coefficient reaches -26.1 × $10^{-6}$ $K^{-1}$[15]. However, previous research primarily focused on tuning the NTE properties of the La(Fe, Si)$_{13}$-based compounds by composition manipulation[16-19], while neglecting their poor mechanical properties. The intrinsic brittleness of La(Fe, Si)$_{13}$-based compounds will result in difficulty in shaping and machining them. Furthermore, their large NTE tends to cause fractures, causing materials and devices to fail[20]. These shortcomings significantly limit the application potential of La(Fe, Si)$_{13}$-based compounds as NTE materials. However, La(Fe, Si)$_{13}$ composites would be ideal candidates for NTE materials if excellent mechanical properties are obtained. Previous work has shown that epoxy resin-bonded magnetocaloric composites exhibit well-improved mechanical properties[21]. Since the epoxy resin exhibits PTE behavior [Supplementary Figure 1], it could be an effective way to obtain tunable NTE as well as high mechanical performance by producing the La(Fe, Si)$_{13}$/resin composites.

In this work, the $La_{0.7}Ce_{0.3}Fe_{11.51}Mn_{0.09}Si_{1.4}$ compound with strong first-order magnetic transition is chosen as an origin NTE material (hereafter refers to La-Fe-Si). Epoxy resin-bonded La-Fe-Si composites were successfully fabricated. The NTE of the La-Fe-Si/resin composites is manipulated by controlling the La-Fe-Si particle size and epoxy resin content. Reducing the particle size will weaken the first-order magnetic transition of the $La_{0.7}Ce_{0.3}Fe_{11.51}Mn_{0.09}Si_{1.4}$ compound, thereby decreasing the NTE of the composites. Tailoring the resin content is a more effective way to tune the NTE of La-Fe-Si/resin composites. The NTE of La-Fe-Si/resin composites gradually decreases as the resin content increases. The La-Fe-Si/resin composite with 20 wt.% resin exhibits ZTE behavior in a wide temperature range. Importantly, the La-Fe-Si/resin composites exhibit high mechanical properties and can maintain mechanical integrity and functional stability after 1000 thermal cycles. As a result, La-Fe-Si/resin composites with tunable NTE, excellent mechanical properties, and long-term cycle stability present great application potential as NTE materials.

## MATERIALS AND METHODS

### Sample preparation

$La_{0.7}Ce_{0.3}Fe_{11.51}Mn_{0.09}Si_{1.4}$ ingot was prepared by induction melting. Then, the ingot was processed into ribbons using the melt-spinning method. The ribbons were subsequently sealed in a quartz tube with an argon atmosphere and annealed at 1393 K for 20 h, followed by ice water quenching. A schematic illustration of $La_{0.7}Ce_{0.3}Fe_{11.51}Mn_{0.09}Si_{1.4}$ powder preparation is shown in Supplementary Figure 2A. The phase composition of the $La_{0.7}Ce_{0.3}Fe_{11.51}Mn_{0.09}Si_{1.4}$ compound is primarily 1:13 phase, accompanied by a very small amount of the $\alpha$-Fe phase and La-rich phase [Supplementary Figure 2B and C]. The annealed $La_{0.7}Ce_{0.3}Fe_{11.51}Mn_{0.09}Si_{1.4}$ ribbons were broken and ground into powders by hand using an agate mortar. Then, the powders were separated into different groups according to their particle sizes using sieves as follows: 280-450 μm, 200-280 μm, 150-200 μm, 75-150 μm, 40-75 μm and < 10 μm. The particle size distribution of these powders was then re-checked by scanning electron microscopy (SEM). As shown in Supplementary Figure 3, the size distribution of these particles obtained from the SEM micrographs of these $La_{0.7}Ce_{0.3}Fe_{11.51}Mn_{0.09}Si_{1.4}$ powders is 397.9, 278.0, 180.4, 96.6, 45.2 and 3.6 μm, respectively (hereafter refers to P398, P278, P180, P97, P45, and P4). The $La_{0.7}Ce_{0.3}Fe_{11.51}Mn_{0.09}Si_{1.4}$ powders were mixed with multiple-component epoxy resin composed of E51 epoxy resin and T31 Mannich amide. The resin-mixed powders were pressed into cylinders of Φ10 mm under a pressure of 900 MPa and then solidified at room temperature for five days. Note that the resin must be precured before pressing for the composites with high resin content to prevent the resin from flowing out of the mold during pressing. The density of these La-Fe-Si/resin composites was estimated using the Archimedes method[12].

### Sample characterization

The temperature-variation X-ray diffraction (XRD) measurement was performed by using Cu *Kα* radiation. The Rietveld refinement was performed on these XRD patterns to identify the phase composition and their crystal structure using the GSAS/EXPGUI software[22]. The microstructure was recorded by SEM, and elemental analysis was performed using energy-dispersive spectroscopy (EDS) equipped with SEM. The three-dimensional (3D) spatial distribution of the different phases of the samples was revealed by using high-resolution X-ray computed tomography (CT). The segmentation and quantitative analysis of the 3D structural images were performed using the Avizo software[23]. Compressive strength was measured by using cylindrical samples of Φ10 × 10 mm by a universal testing machine under ambient temperature. Magnetic measurements were performed using a vibrating sample magnetometer (VSM, Quantum Design, VersaLab). The differential scanning calorimetry (DSC) measurements were carried out using DSC 6220 with a ramp rate of 10 K/min. The linear thermal expansion ($\Delta L/L$) was measured using a thermo-dilatometer with a heating rate of 2 K/min.

## RESULTS AND DISCUSSION

### Tunable NTE via adjusting particle size

The NTE of La(Fe, Si)$_{13}$ compounds is closely related to the magnetic transition. The thermal and magnetic hysteresis decrease gradually with reducing particle size [Supplementary Figures 4 and 5], which implies the weakening of the first-order magnetic transition. The reduction in thermal and magnetic hysteresis can be ascribed to the partially-removed internal strain and grain boundaries as well as the significantly increased specific surface areas of the samples [Supplementary Figures for detailed analysis]. The weakening of first-order magnetic transition can also be confirmed by the Arrott plots [Supplementary Figure 6]. Moreover, the magnetic entropy change ($\Delta S_M$) decreases gradually with reducing particle size owing to the weakening of the first-order magnetic transition [Supplementary Figure 7]. The maximum -$\Delta S_M$ value of the ribbon samples can reach as high as 21.5 J/kg K under a low magnetic field change of 0-1 T, and the La-Fe-Si powders with an average particle size of ~4 μm can still exhibit a giant magnetic entropy change of 10.1 J/kg K. This implies the strong first-order magnetic transition of the $La_{0.7}Ce_{0.3}Fe_{11.51}Mn_{0.09}Si_{1.4}$ compound. The strong first-order magnetic transition enables the La-Fe-Si compound to exhibit excellent NTE properties. The average CTE of the La-Fe-Si compound obtained from the temperature-variation XRD can reach -76.4 × $10^{-6}$ $K^{-1}$ in the NTE region from 100 K to 180 K [Supplementary Figure 8].

To optimize the NTE properties of the La-Fe-Si/resin composites, 3 wt.% epoxy resin was mixed with the $La_{0.7}Ce_{0.3}Fe_{11.51}Mn_{0.09}Si_{1.4}$ powders of different particle sizes to produce a series of composites. The backscattered electron (BSE) image of a fabricated La-Fe-Si/resin composite with 3 wt.% resin and the corresponding elemental mapping of La, Ce, Fe, Mn, Si and C elements are shown in Supplementary Figure 9. La, Ce, Fe, Mn and Si elements are homogeneously distributed in the $La_{0.7}Ce_{0.3}Fe_{11.51}Mn_{0.09}Si_{1.4}$ particles, and the C originates from the epoxy resin. Figure 1A shows the BSE images of the P398, P278, P180, P97, P45 and P4 composites. The La-Fe-Si particle size gradually decreases in the P398 to P4 samples. The epoxy resin (black areas) with high fluidity is uniformly distributed around the particle boundaries and among their narrow gaps. The composites exhibit a denser microstructure with reduced particle sizes. Reducing the particle size could increase the surface area of the particles, so particles with smaller sizes can contact with the epoxy resin by a larger surface area, and hence, the total bonding force between La-Fe-Si particles and resin is enhanced. Namely, the La-Fe-Si/resin composites with smaller particle sizes have a denser structure in the case of the same amount of epoxy resin used. Moreover, a dense structure improves NTE and the mechanical properties of the La-Fe-Si/resin composites. The BSE and secondary electron (SE) images of the P180 composite are shown in Supplementary Figure 10. The resin regions and pores are present as black areas in the BSE image, but from the SE image, the pores are darker and bigger areas than the resin regions. The distribution of pores and resin will be further distinguished later by elemental mapping. To further study the densification of La-Fe-Si/resin composites with different particle sizes, the porosity of La-Fe-Si/resin composites with different particle sizes can be estimated using the following equation: porosity = $(\rho_{the} - \rho_{exp})/\rho_{the}$, where $\rho_{the}$ and $\rho_{exp}$ represent theoretical density and experimental density, respectively; $\rho_{the}$ is calculated by $\rho_{the} = \rho_{La\text{-}Fe\text{-}Si}$ × La-Fe-Si content + $\rho_{resin}$ × resin content, whereas $\rho_{exp}$ is obtained using the Archimedes method. Figure 1B displays the porosity of La-Fe-Si/resin composites with different particle sizes. As the particle size decreases, the porosity of the composites first decreases from P398 to P180 samples, and then, porosity increases with reducing particle size. As mentioned above, the increasing surface areas of particles caused by the reduction in particle size can improve the densification of composites, thereby decreasing porosity at first. Nevertheless, while further reducing the particle size, the particles with smaller sizes are more likely to agglomerate during mixing. As shown in Figure 1A, fine La-Fe-Si particles with an average diameter of ~4 μm tend to clump together, forming many large epoxy resin regions in the La-Fe-Si/resin composites. In addition, with an increase in surface areas, more resin is required to cover all particle surfaces. Therefore, 3 wt.% epoxy resin may not be sufficient to cover the surface of all La-Fe-Si particles to bond them, thus leading to the formation of more pores. Consequently, once the average particle size is smaller than 180 μm, the porosity of composites

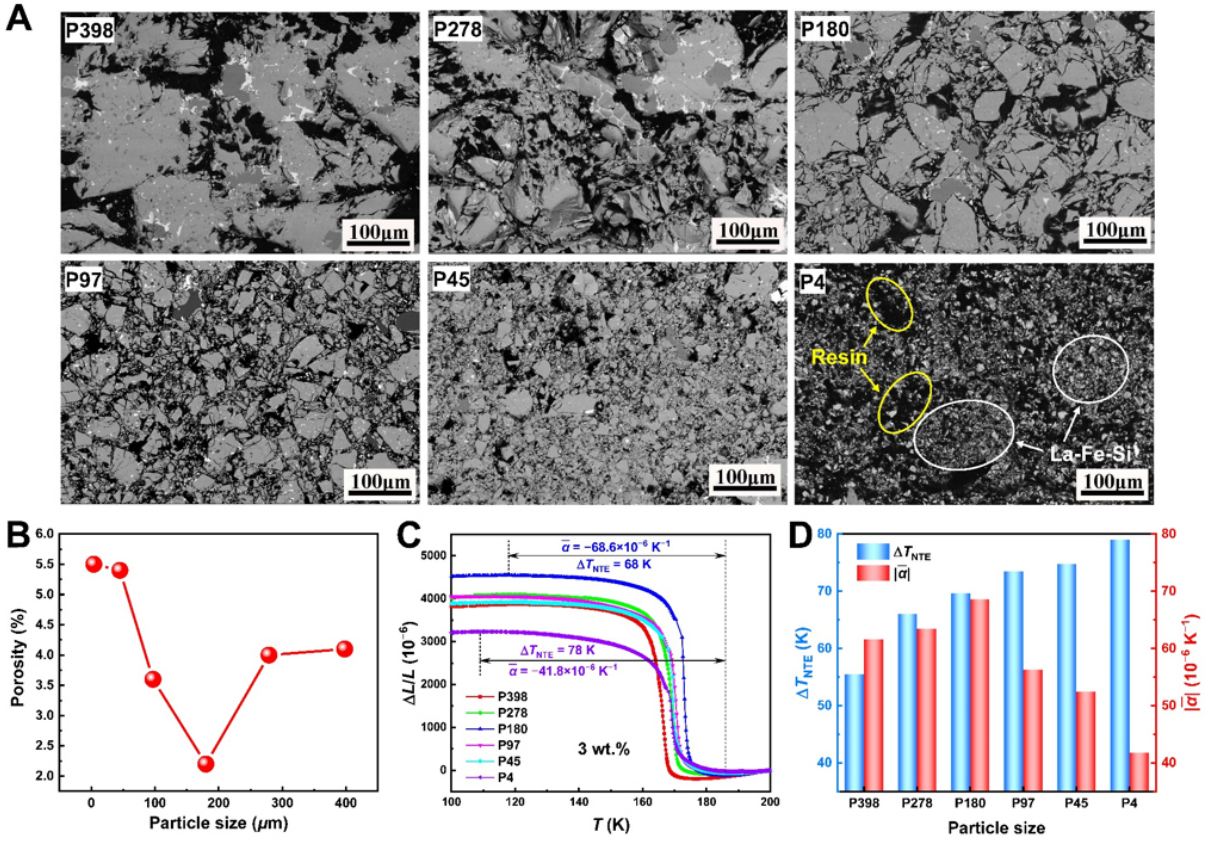


**Figure 1.** (A) BSE images of La-Fe-Si/resin composites with different particle sizes; (B) porosity of La-Fe-Si/resin composites with different particle sizes; (C) temperature dependence of linear thermal expansion ($\Delta L/L$) for La-Fe-Si/resin composites with different particle sizes; (D) NTE temperature range and average linear NTE coefficient of La-Fe-Si/resin composites with different particle sizes. BSE: Backscattered electron; NTE: negative thermal expansion.

increases with the further reduction in particle size.

Figure 1C presents the temperature dependence of the linear thermal expansion ($\Delta L/L$) of the La-Fe-Si/resin composites with 3 wt.% resin content with different particle sizes (the reference temperature is 200 K). The linear thermal expansion increases as the temperature decreases, which indicates the NTE of the La-Fe-Si/resin composites. Furthermore, the NTE property varies distinctly with the reduction in particle size. The NTE temperature region ($\Delta T_{NTE}$) in which the composites exhibit NTE behavior and the average linear coefficient of thermal expansion ($\bar{\alpha} = \frac{(\Delta L/L)_{T_2} - (\Delta L/L)_{T_1}}{T_2 - T_1}$) in the $\Delta T_{NTE}$ as a function of particle size are shown in Figure 1D. $\Delta T_{NTE}$ increases monotonously with reducing particle size. As mentioned above, reducing particle size will weaken the first-order magnetic transition of the $La_{0.7}Ce_{0.3}Fe_{11.51}Mn_{0.09}Si_{1.4}$ compound. Therefore, the magnetic transition will become less sharp; that is, the transition temperature window will be widened. Unlike the monotonous variation of $\Delta T_{NTE}$, $\bar{\alpha}$ first increases gradually with the reduction in particle size while the average particle size is larger than 180 μm. However, $\bar{\alpha}$ decreases remarkably with the reduction in particle size as the particle size is further reduced, which is consistent with the opposite variation trend of porosity [Figure 1B]. We assume that the reduction in particle size would lead to two effects on the NTE of La-Fe-Si/resin composites. First, the first-order magnetic transition will be weakened by reducing the particle size, thereby leading to a lower $\bar{\alpha}$; second, the reduction in particle size decreases or

increases porosity [Figure 1B], which would then increase or decrease $\bar{\alpha}$. When the average particle size is larger than 180 μm, the reduction in particle size weakens the first-order magnetic transition as well as lowers porosity, which has opposite effects on the NTE of La-Fe-Si/resin composites. The increase in $\bar{\alpha}$ implies that the latter factor plays a predominant role. When the particle size is further reduced to lower than 180 μm, both weakening of first-order magnetic transition and an increase in porosity will lower the NTE of La-Fe-Si/resin composites, thereby decreasing $\bar{\alpha}$. This result suggests that porosity is a more important factor that affects the NTE of La-Fe-Si/resin composites. Among the composites, the P180 composite exhibits the highest NTE property because it has the lowest porosity. Its $\bar{\alpha}$ is estimated to be -68.6 × $10^{-6}$ $K^{-1}$ in the NTE temperature region from 120 to 185 K, which can be comparable to those of some typical NTE materials, such as $Fe_{41.5}Mn_{28}Ga_{30.5}$ (-59.8 × $10^{-6}$ $K^{-1}$, 136-220 K)[24], $LaFe_{11.2}Al_{1.3}Si_{0.5}$ (-28.3 × $10^{-6}$ $K^{-1}$, 150-200 K)[25], $Mn_{0.97}In_{0.03}CoGe$ (-66.6 × $10^{-6}$ $K^{-1}$, 58-230 K)[5], and $Ag_{0.5}NMn_{3.5}$ (-5.14 × $10^{-6}$ $K^{-1}$, 135-185 K)[26]. When the average particle size decreases to ~4 μm, the P4 composite can still obtain a large $\bar{\alpha}$ of -41.8 × $10^{-6}$ $K^{-1}$. These results demonstrate that controlling the particle size is an effective way to tune the NTE of La-Fe-Si/resin composites. However, by only tuning the La-Fe-Si particle size, it is very difficult to reach precisely tailored NTE properties, and a ZTE case can barely be achieved.

### Microstructure of La-Fe-Si/resin composites

Owing to the excellent NTE performance of the P180 composite, the P180 powder is chosen to further optimize La-Fe-Si/resin composites with different resin contents to better tune their NTE and to obtain ZTE composites. The proportions of the epoxy resin are 3, 10, 20, 30, 40, 50, 60, 70 and 80 wt.%, respectively (hereafter refers to Resin3, Resin10, Resin20, Resin30, Resin40, Resin50, Resin60, Resin70, and Resin80). The La-Fe-Si/resin composites are composed of La-Fe-Si phase and resin, and no impurity phase is observed, indicating that the pressing process does not cause the instability of the La-Fe-Si phase [Supplementary Figure 11]. Figure 2A shows the optical morphologies of La-Fe-Si/resin composites with different resin contents. As shown in the magnified image of the Resin80 composite, the white areas represent $La_{0.7}Ce_{0.3}Fe_{11.51}Mn_{0.09}Si_{1.4}$ particles, and the gray areas represent the epoxy resin. The composite gradually changes from metallic luster to a transparent state when the epoxy resin content increases from 3 wt.% to 80 wt.%, indicating that the matrix of La-Fe-Si/resin composites changes from La-Fe-Si powders to epoxy resin. When the epoxy resin content is 3 wt.%, the epoxy resin is used as a binder to bond La-Fe-Si particles. Conversely, when the epoxy resin content is more than the La-Fe-Si content, the epoxy resin will wrap La-Fe-Si particles; that is, La-Fe-Si particles are evenly distributed in the resin matrix. This structure can increase the densification of La-Fe-Si/resin composites, thereby improving their mechanical properties. In addition, the DSC curves of La-Fe-Si powders and La-Fe-Si/resin composites indicate that the La-Fe-Si powders and composites with different resin contents exhibit consistent DSC peaks, which implies that the epoxy resin will not affect the first-order magnetic transition of La-Fe-Si compound. However, the Resin20 and Resin80 composites show wider DSC peaks, which may be attributed to the poor thermal conductivity of the Resin20 and Resin80 composites [Supplementary Figure 12].

Figure 2B shows the BSE images of La-Fe-Si/resin composites with different resin contents. The gray areas represent the La-Fe-Si phase, and the black areas represent the epoxy resin and pores. La-Fe-Si particles have a homogeneous particle size, and the epoxy resin is primarily distributed among La-Fe-Si particles because of high fluidity. Moreover, La-Fe-Si particles are uniformly distributed in the epoxy resin matrix without segregation. When the resin content reaches 80 wt.%, the resin will become the matrix of La-Fe-Si/resin composites, whereas La-Fe-Si particles will be the additive phase. Therefore, the La-Fe-Si/resin composite is presumed to exhibit positive thermal expansion.

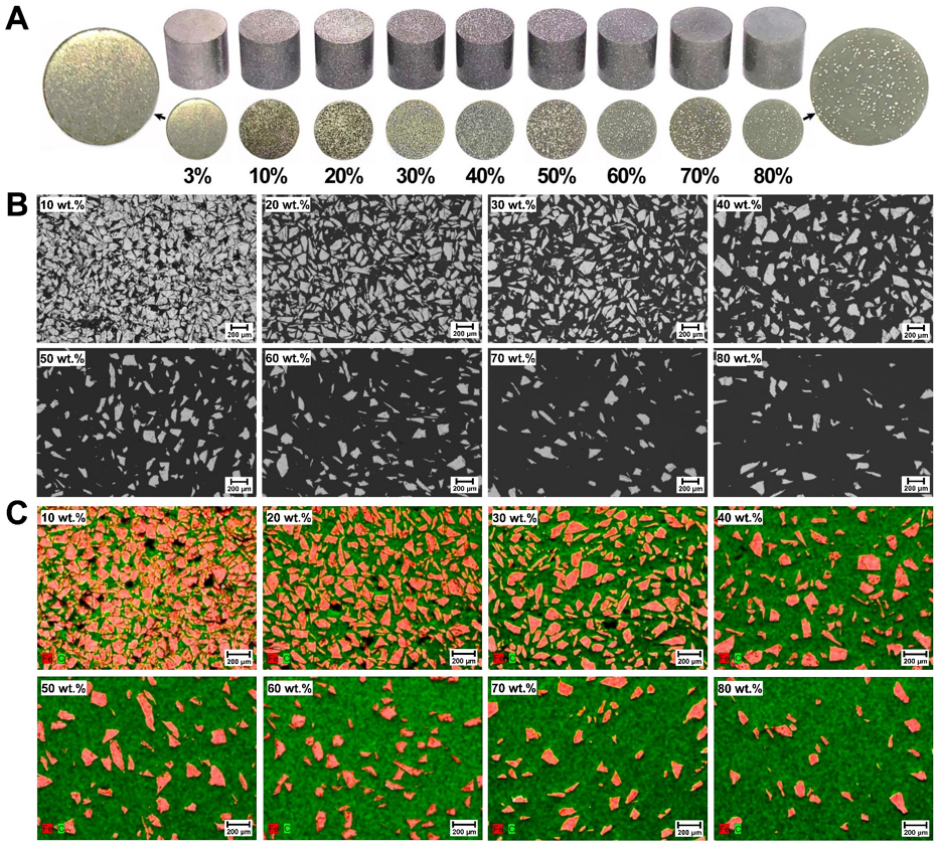


**Figure 2.** (A) Images of La-Fe-Si/resin composites with different resin contents; (B) BSE images of La-Fe-Si/resin composites with different resin contents; (C) elemental mapping of Fe and C for La-Fe-Si/resin composites with different resin contents. BSE: Backscattered electron.

Since both the epoxy resin and pores are represented as black areas in the obtained SEM images, to further distinguish the epoxy resin and pores, the elemental mapping of Fe and C in La-Fe-Si/resin composites is performed and shown in Figure 2C. The orange areas (Fe element) represent $La_{0.7}Ce_{0.3}Fe_{11.51}Mn_{0.09}Si_{1.4}$ particles, the green areas (C element) represent the epoxy resin, and the black areas represent the pores. A large number of pores can be observed in the Resin10 composite, and these pores are primarily distributed in the particle boundaries. With an increase in resin content, the number of pores gradually decreases and eventually disappears when the resin content is greater than 30 wt.%. For La-Fe-Si/resin composites, increasing epoxy resin content will fill more pores during compressing, thereby decreasing porosity and improving densification. Such a compact structure improves mechanical and NTE properties. Moreover, during the SEM sample preparation, sanding may cause La-Fe-Si particles to fall off the La-Fe-Si/resin composites, leading to the appearance of pores in the La-Fe-Si/resin composites. With increasing resin content, the disappearance of pores further indicates the enhancement of the bonding force between the epoxy resin and La-Fe-Si particles.

High-resolution X-ray CT is performed to further investigate the internal spatial structure of La-Fe-Si/resin composites. Figure 3A-C show the 3D rendered volume images of each component for Resin3, Resin20 and Resin80 composites, respectively. A central region with a volume of 1000 × 1000 × 1000 $\mu m^3$ of the sample was chosen for 3D rendering and analysis. The blue parts represent La-Fe-Si particles, the red parts represent the epoxy resin, and the green parts represent pores. The leftmost full 3D structural images in

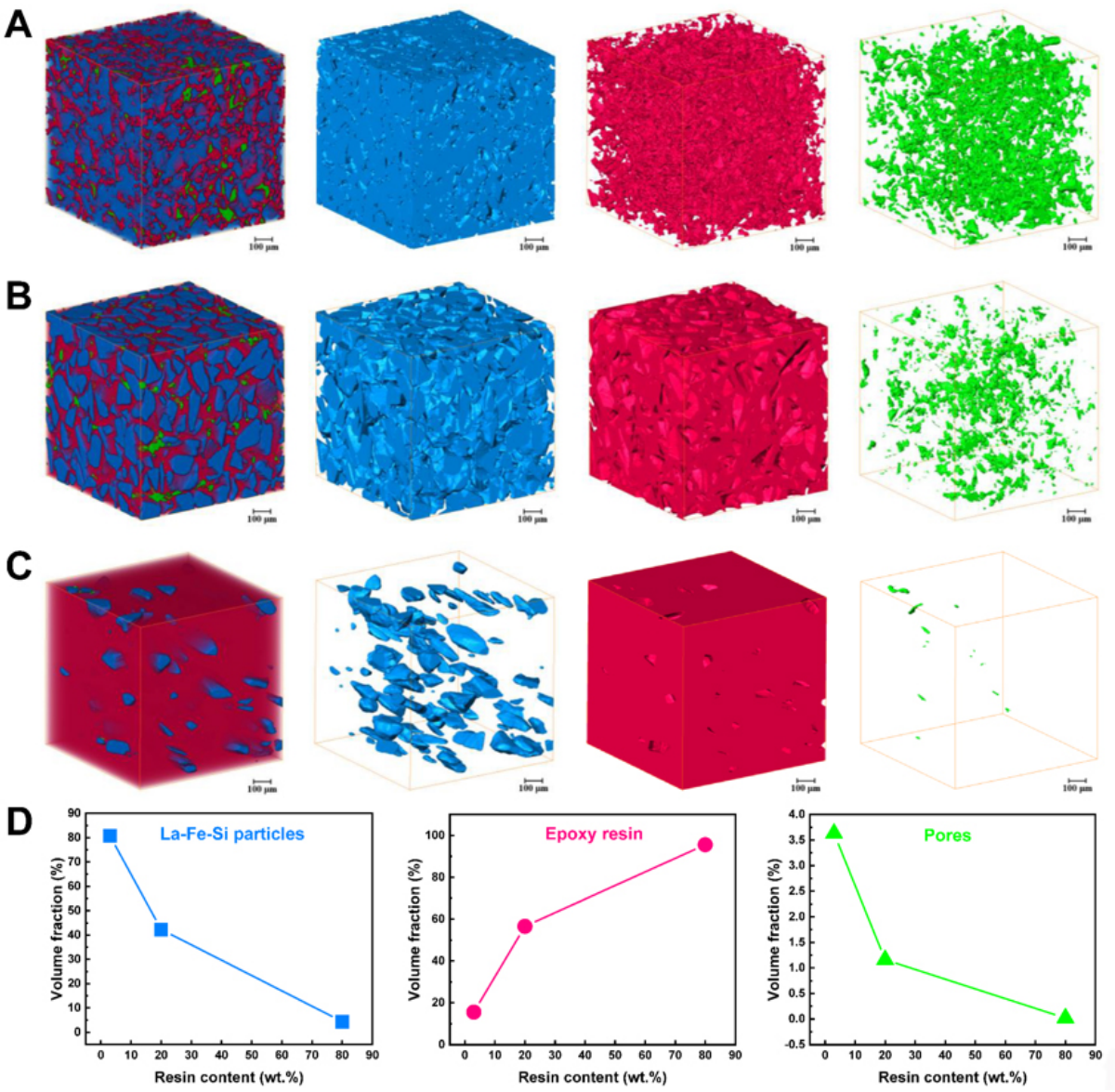


**Figure 3.** 3D rendering images of each phase for (A) Resin3; (B) Resin20; and (C) Resin80 composites. From left to right: the overlapping configuration, La-Fe-Si phase, epoxy resin and pores; (D) volume fraction of La-Fe-Si particle, epoxy resin and pore.

Figure 3A-C show that the resin (red region) tends to be among La-Fe-Si particles (blue region) and dispersive pores (green region). The stereo structure of La-Fe-Si particles, resin and pores reveals the homogeneity of the spatial structure. For the Resin3 composite, the resin exists in an irregular shape due to high fluidity. With increasing resin content, the resin will wrap La-Fe-Si particles and further fill the pores. According to the quantitative analysis of the Avizo software, the volume fraction of each component in the composites is obtained and shown in Figure 3D. The volume fractions of the epoxy resin in Resin3, Resin20 and Resin80 composites are 15.54 %, 56.55 % and 95.57 %, respectively. Since the epoxy resin exhibits PTE behavior, an increase in resin fraction would lower the NTE of the La-Fe-Si/resin composites, exhibiting ZTE behavior at a certain resin content. In addition, further resin addition will fill the pores, improving densification; for example, the porosity of the Resin3, Resin20 and Resin80 composites is determined to be 3.63%, 1.16% and 0.02%, respectively. The denser the structure of La-Fe-Si/resin composites, the better their

mechanical properties.

### High mechanical properties

Figure 4A presents the compressive stress-strain curves of the Resin3, Resin20, and Resin80 composites. Note that the stress-strain curve of the pure $La_{0.7}Ce_{0.3}Fe_{11.51}Mn_{0.09}Si_{1.4}$ compound cannot be obtained because it is in the form of ribbons. According to previous reports, the compressive stress-strain curves of bulk La-Fe-Si compounds drop sharply without further plastic deformation[27], indicating the brittleness of these compounds. Nevertheless, the Resin3 composite exhibits a short yield stage before reaching the maximum compressive strength [Figure 4A], which is due to the densification of the porous architecture under stress. With increasing resin content, more pores can be filled, thereby reinforcing the binding force between La-Fe-Si particles. As a result, the compressive strength increases gradually with increasing resin content. The Resin80 composite exhibits compressive strength of 205 MPa, which is 75% higher than that of the Resin3 composite. The enhanced mechanical properties guarantee the integration of materials when La-Fe-Si/resin composites are used as NTE materials. Moreover, the obtained Resin20 composite can be easily machined into different shapes for practical applications, such as thin plates, strips, and rods, as shown in Figure 4B. In addition, Figure 4C shows the temperature dependence of thermal conductivity for Resin3 composite. It can be found that the Resin3 composite shows relatively high thermal conductivity, which can be comparable with some pure $La(Fe, Si)_{13}$-based compounds[15,28]. This facilitates the practical application of the composites as NTE materials.

### Tunable NTE via adjusting resin contents

Figure 5A presents the temperature dependence of linear thermal expansion ($\Delta L/L$) for La-Fe-Si/resin composites with different resin contents. With increasing resin contents, La-Fe-Si/resin composites exhibit a distinct decrease in NTE, which is more remarkable than that tuned by particle size as observed in Figure 1C. The $\Delta L/L$ below $T_C$ gradually changes from a large positive value to a large negative value, which confirms our speculation that the resin with PTE will compensate for the NTE of La-Fe-Si particles, thereby gradually tuning La-Fe-Si/resin composites from NTE materials to PTE materials. This result also proves that adjusting the resin content is more effective for adjusting the NTE of La-Fe-Si/resin composites than adjusting the La-Fe-Si particle size. Note that the Resin20 composite exhibits ZTE behavior in a wide temperature range below $T_C$. The $\bar{\alpha}$ of the Resin20 composite is estimated to be $0.8 \times 10^{-6}$ $K^{-1}$ in the temperature range of 100-165 K, which is comparable to other ZTE materials, such as $LaFe_{10.0}Si_{3.0}C_{0.4}$ ($-0.4 \times 10^{-6}$ $K^{-1}$, 120-229 K)[29], $Gd_{0.25}Dy_{0.75}Co_{1.93}Fe_{0.07}$ ($-0.61 \times 10^{-6}$ $K^{-1}$, 98-270 K)[30] and $Tb(Co_{1.9}Fe_{0.1})$ ($0.48 \times 10^{-6}$ $K^{-1}$, 123-307 K)[31]. Although composites with high resin content exhibit a distinct PTE behavior below $T_C$, the NTE property can still be observed around $T_C$, even in the Resin80 composite. The $\bar{\alpha}$ of the Resin80 composite is $-8.1 \times 10^{-6}$ $K^{-1}$ in the NTE temperature range from 168 K to 180 K. This fact suggests the strong intrinsic NTE property of La-Fe-Si compound due to the magnetic transition from the PM phase with a small lattice to the FM phase with a large lattice.

Figure 5B shows the NTE temperature region as a function of the resin content. The wide NTE temperature region from 118 K to 186 K for the Resin3 composite indicates that the $La_{0.7}Ce_{0.3}Fe_{11.51}Mn_{0.09}Si_{1.4}$ compound not only exhibits a significant NTE property around $T_C$, but also exhibits NTE behavior in a wide temperature range below $T_C$. This NTE below $T_C$ can be confirmed by the variation of $\Delta a/a$ as shown in Supplementary Figure 8C. This fact also suggests that there still exists strong magnetoelastic coupling below $T_C$ for the $La_{0.7}Ce_{0.3}Fe_{11.51}Mn_{0.09}Si_{1.4}$ compound. With increasing resin content, the lower limit temperature of NTE increases largely, whereas the upper limit temperature gradually decreases. In particular, the NTE temperature range decreases significantly from 68 K for the Resin3 composite to 19 K for the Resin30 composite. The significant increase in the lower limit temperature suggests that the NTE below $T_C$ caused by

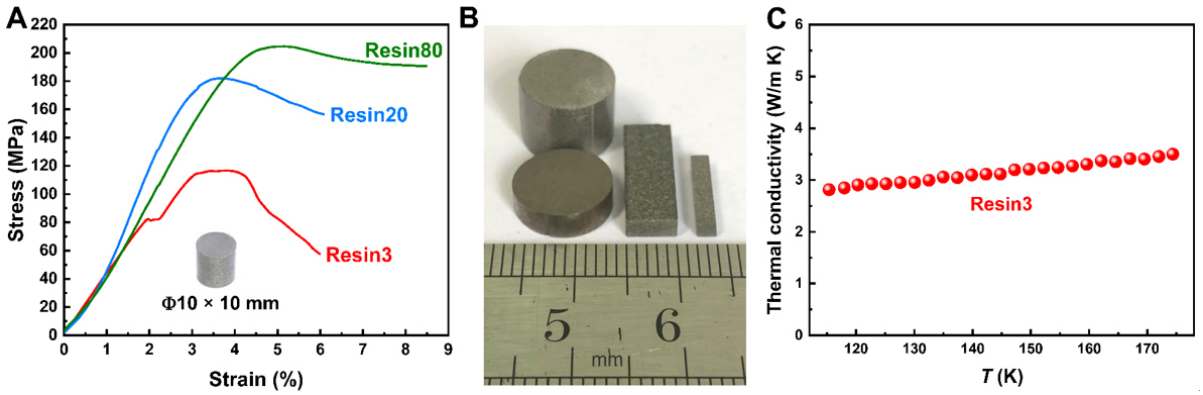


**Figure 4.** (A) Compressive stress-strain curves for Resin3, Resin20 and Resin80 composites; (B) different shapes machined from the Resin20 composite; (C) temperature dependence of thermal conductivity for Resin3 composite.

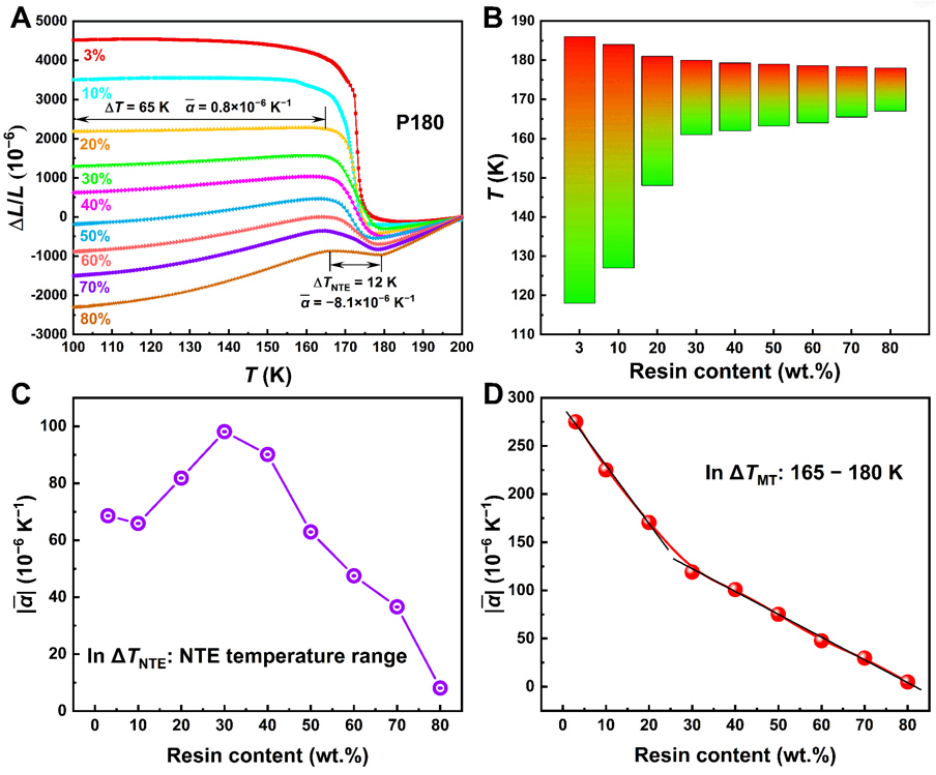


**Figure 5.** (A) Temperature dependence of linear thermal expansion ($\Delta L/L$) for La-Fe-Si/resin composites with different resin contents; (B) NTE temperature range as a function of resin content; Average linear NTE coefficient as a function of resin content in the (C) NTE temperature range and (D) magnetic transition temperature range. NTE: Negative thermal expansion.

the magnetoelastic coupling is compensated by the PTE of the resin. However, the NTE originating from the magnetic transition is significantly stronger; thus, the NTE temperature region remains until the resin content even reaches 80 wt.%.

Figure 5C shows the average NTE coefficient of La-Fe-Si/resin composites with different resin contents in their respective NTE temperature ranges ($\Delta T_{NTE}$). The average NTE coefficient of the La-Fe-Si/resin composites increases and then decreases with increasing resin content. Similarly, an increase in resin

content also has two opposite effects on the average NTE coefficient. First, increasing the resin content can improve the densification of composites, thereby improving NTE; second, the PTE of the epoxy resin will compensate for the NTE of La-Fe-Si particles, decreasing NTE. This result suggests that the first effect plays a predominant role if the resin content is lower than 30 wt.%, whereas the second effect becomes more prominent if the resin content is higher than 30 wt.%. Furthermore, the average NTE coefficient of the La-Fe-Si/resin composites with different resin contents in the magnetic transition temperature range ($\Delta T_{MT}$: 165-180 K) is determined to further investigate the variation of NTE during the phase transition, as shown in Figure 5D. $\bar{\alpha}$ first decreases significantly from -275.0 × $10^{-6}$ $K^{-1}$ for the Resin3 composite to -119.0 × $10^{-6}$ $K^{-1}$ for the Resin30 composite, and then, the slope becomes lower, and $\bar{\alpha}$ decreases gradually to -4.9 × $10^{-6}$ $K^{-1}$ for the Resin80 composite. As mentioned above, the PTE of the resin and pores in the composites can weaken the NTE of the composites. Figure 2C shows that the number of pores gradually decreases as the resin content increases; for example, porosity decreases from the Resin3 composite's 3.63% to the Resin20 composite's 1.16% [Figure 3D]. Then, the pores in the composites almost disappear [Figure 2C]. This reveals that the NTE of La-Fe-Si/resin composites will be less affected by pores if the resin content is more than 20 wt.%, thereby leading to the change of slope. In addition, although the resin has become the matrix of the La-Fe-Si/resin composites when the resin content reaches 80 wt.%, the Resin80 composite still exhibits significant NTE in the magnetic transition temperature range. This result further proves the strong intrinsic NTE properties of the $La_{0.7}Ce_{0.3}Fe_{11.51}Mn_{0.09}Si_{1.4}$ compound during the PM-FM magnetic transition. Furthermore, the theoretical thermal expansion of La-Fe-Si/resin composites with different resin contents can be obtained based on the thermal expansion of the epoxy resin and La-Fe-Si compound [Supplementary Figure 13A]. Then, the coefficient of thermal expansion of La-Fe-Si/resin composites with different resin contents can be calculated. The experimental and theoretical values of coefficients of thermal expansion of the composites in the magnetic transition temperature range are shown in Supplementary Figure 13B. It can be seen that both theoretical and experimental values gradually decrease with the increase of resin content. Moreover, the experimental values are lower than the theoretical values. The thermal expansion obtained from the temperature-variation XRD measurement may deviate from the actual thermal expansion of the La-Fe-Si compound. In addition, the existence of pores in the composites will affect the thermal expansion of the composites. Therefore, the experimental values of coefficients of thermal expansion are different from the theoretical values.

### Long-term cycle stability

The strong NTE behavior, particularly the remarkable NTE during the magnetic transition, can cause microcracks in La-Fe-Si/resin composites during their cycling service due to the repeated shrinkage and expansion, leading to material failure. Therefore, long-term cycle stability is a vital prerequisite for the applications of NTE materials. Here, the Resin3 composite is chosen to conduct the thermal cycle test around the transition temperature. As shown in Figure 6A, the Resin3 composite is thermally cycled in liquid nitrogen and hot water (~358 K) to investigate its cycle stability. Figure 6B shows that the Resin3 composite still maintains decent integrity after 1000 thermal cycles, which means that it has excellent mechanical properties. Figure 6B shows the surface morphology obtained by optical microscopy and SEM before and after 1000 thermal cycles. After undergoing 1000 thermal cycles, the Resin3 composite maintains its original macro- and micro-structure without significant differences and does not exhibit any visible cracks, which suggests that La-Fe-Si/resin composites have long-term cycle stability. In addition, Figure 6C compares the compressive stress-strain curves of the Resin3 composite before and after the thermal cycle test. It can be found that the compressive strength of the Resin3 composite after cycle stability test is 119.9 MPa, which is close to that of Resin3 composite before cycle stability test (116.6 MPa). Therefore, the mechanical properties of the composites do not show significant changes after the long-term cycle stability test.

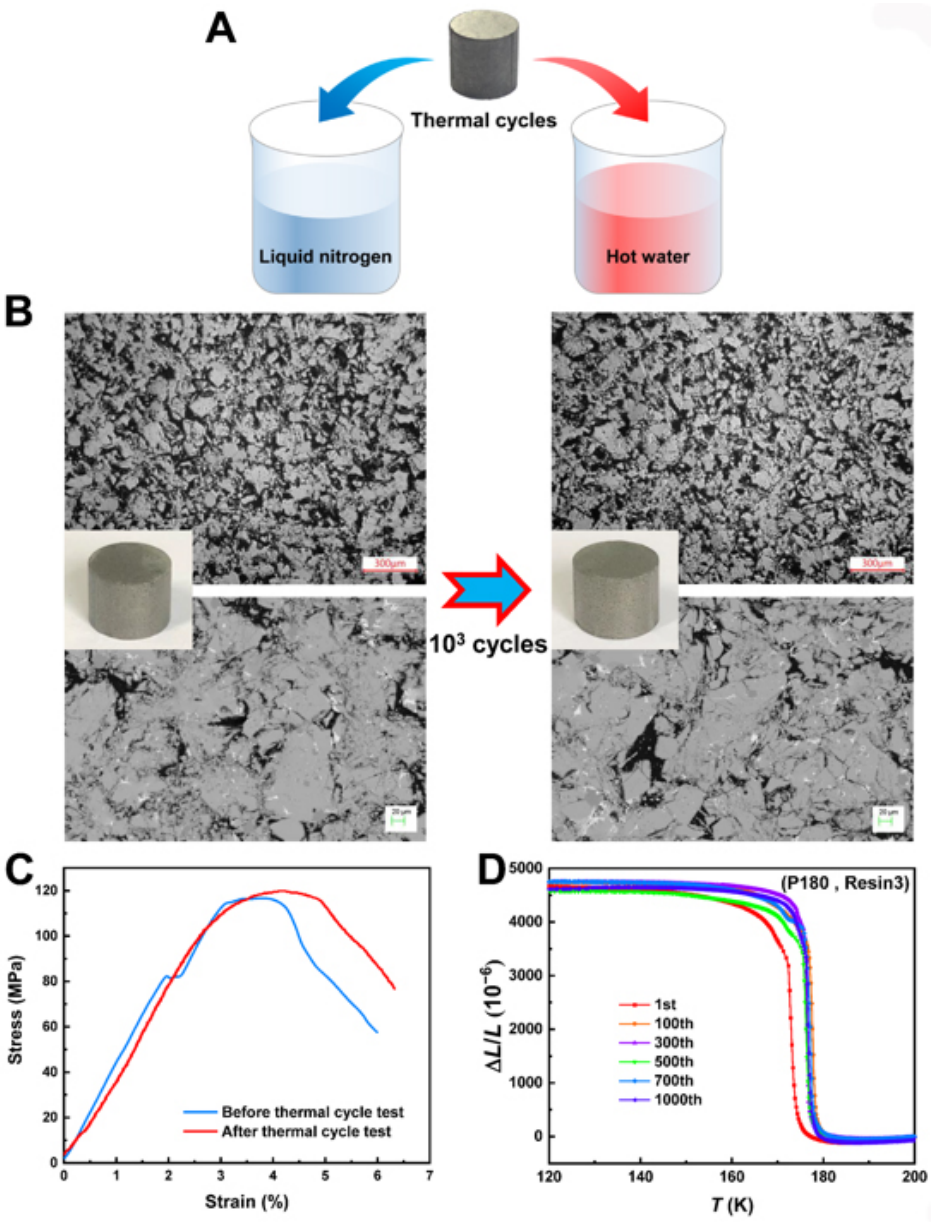


**Figure 6.** (A) Schematic illustration of thermal cycles; (B) surface morphology (upper) and SEM images (lower) of the Resin3 composite before and after 1000 thermal cycles; (C) compressive stress-strain curves of the Resin3 composite before and after cycle stability test; (D) temperature dependence of linear thermal expansion ($\Delta L/L$) for the Resin3 composite at the selected thermal cycles. SEM: Scanning electron microscopy.

Figure 6D shows the temperature dependence of the linear thermal expansion ($\Delta L/L$) for the Resin3 composite at some selected cycles. Note that the transition temperature increases after the first cycle. For La(Fe, Si)$_{13}$ compounds, the hydrostatic pressure can change the curve of the free energy $E(M, T)$ by the renormalization effect of spin fluctuations, thereby decreasing $T_C$[32]. Moreover, the internal constraints can also reduce the $T_C$[33]. Since La-Fe-Si/resin composites are prepared by compaction, the residual stress after the compaction and constraints from the surrounding epoxy resin will decrease the transition temperature of the $La_{0.7}Ce_{0.3}Fe_{11.51}Mn_{0.09}Si_{1.4}$ compound. During the thermal cycle, the cyclic MVE will drive $La_{0.7}Ce_{0.3}Fe_{11.51}Mn_{0.09}Si_{1.4}$ particles to shrink and expand repeatedly. This process will gradually release the residual stress

and surrounding constraints, increasing the transition temperature. After the 100th cycle, the release of residual stress and constraints is completed; thus, the transition temperature will no longer change. In addition, the NTE performance of the Resin3 composite undergoing different thermal cycles does not exhibit obvious variations, which proves its robust functional stability. These results strongly suggest that the fabricated La-Fe-Si/resin composites are highly suitable for practical applications as NTE materials.

## CONCLUSIONS

In summary, epoxy resin-bonded La-Fe-Si/resin composites are fabricated, and their NTE is tuned by controlling the La-Fe-Si particle size and epoxy resin content. The reduction in particle size weakens the first-order magnetic transition of the $La_{0.7}Ce_{0.3}Fe_{11.51}Mn_{0.09}Si_{1.4}$ compound, which reduces NTE and the thermal/magnetic hysteresis. Meanwhile, the reduction in particle size first decreases porosity, which increases NTE until the average particle size of 180 μm. Then, the NTE decreases significantly with a further reduction in particle size caused by the weakening of the first-order magnetic transition and the increase in porosity. Furthermore, tailoring the epoxy resin content can tune the NTE of La-Fe-Si/resin composites more effectively. An increase in resin content also has two opposite effects on NTE. The La-Fe-Si/resin composite with 80 wt.% resin still exhibits significant NTE during the magnetic transition, which suggests that the $La_{0.7}Ce_{0.3}Fe_{11.51}Mn_{0.09}Si_{1.4}$ compound has strong NTE properties because of its magnetoelastic coupling effect. Moreover, the La-Fe-Si/resin composite with 20 wt.% resin exhibits ZTE behavior in a wide temperature range. Further microstructure analysis indicates that increasing the resin content can fill more pores, leading to a compact structure and enhancing the mechanical properties significantly. La-Fe-Si/resin composites can still maintain their mechanical integrity and excellent NTE properties after 1000 thermal cycles, which proves their excellent cycle stability. Consequently, with the excellent mechanical properties, durable cycle stability, and tunable NTE properties, the fabricated epoxy resin-bonded La-Fe-Si/resin composites could be an attractive candidate for NTE materials.

## DECLARATIONS

### Authors' contributions

Conceived the idea: Zhang H
Performed the experiments and data analysis: Zhou H, Liu Y, Xia M, Yu Z, Chen H, Qiao K, Cong J
Provided the technical support: Huang R, Chen B, Taskaev SV, Chu K
Wrote the manuscript: Zhou H, Zhang H

### Availability of data and materials

Not applicable.

### Financial support and sponsorship

This work was supported by the National Natural Science Foundation of China (Grant Nos.: 52171169, 52101210, 51971160, and 52142305); the National Key Research and Development Program of China (Grant No.: 2021YFB3501204); the Fundamental Research Funds for the Central Universities and the Youth Teacher International Exchange & Growth Program (Grant Nos.: FRF-GF-20-08B and QNXM20210014).

### Conflicts of interest

All authors declared that there are no conflicts of interest.

### Ethical approval and consent to participate

Not applicable.

### Consent for publication

Not applicable.



## REFERENCES

1. Evans JSO, Hu Z, Jorgensen JD, Argyriou DN, Short S, Sleight AW. Compressibility, phase transitions, and oxygen migration in zirconium tungstate, $ZrW_2O_8$. *Science* 1997;275:61-5. DOI PubMed
2. Mary TA, Evans JSO, Vogt T, Sleight AW. Negative thermal expansion from 0.3 to 1050 kelvin in $ZrW_2O_8$. *Science* 1996;272:90-2. DOI
3. Iikubo S, Kodama K, Takenaka K, Takagi H, Takigawa M, Shamoto S. Local lattice distortion in the giant negative thermal expansion material $Mn_3Cu_{1-x}Ge_xN$. *Phys Rev Lett* 2008;101:205901. DOI PubMed
4. Gao Q, Wang J, Sanson A, et al. Discovering large isotropic negative thermal expansion in framework compound $AgB(CN)_4$ via the concept of average atomic volume. *J Am Chem Soc* 2020;142:6935-9. DOI PubMed
5. Zhao YY, Hu FX, Bao LF, et al. Giant negative thermal expansion in bonded MnCoGe-based compounds with $Ni_2In$-type hexagonal structure. *J Am Chem Soc* 2015;137:1746-9. DOI PubMed
6. Katayama N, Otsuka K, Mitamura M, Yokoyama Y, Okamoto Y, Takenaka K. Microstructural effects on negative thermal expansion extending over a wide temperature range in $\beta$-$Cu_{1.8}Zn_{0.2}V_2O_7$. *Appl Phys Lett* 2018;113:181902. DOI
7. Song Y, Shi N, Deng S, Xing X, Chen J. Negative thermal expansion in magnetic materials. *Progr Mater Sci* 2021;121:100835. DOI
8. Li CW, Tang X, Muñoz JA, et al. Structural relationship between negative thermal expansion and quartic anharmonicity of cubic $ScF_3$. *Phys Rev Lett* 2011;107:195504. DOI PubMed
9. Chen J, Xing X, Sun C, et al. Zero thermal expansion in $PbTiO_3$-based perovskites. *J Am Chem Soc* 2008;130:1144-5. DOI PubMed
10. Shen BG, Sun JR, Hu FX, Zhang HW, Cheng ZH. Recent Progress in exploring magnetocaloric materials. *Adv Mater* 2009;21:4545-64. DOI
11. Liu Y, Fu X, Yu Q, Zhang M, Liu J. Significant reduction of phase-transition hysteresis for magnetocaloric $(La_{1-x}Ce_x)_2Fe_{11}Si_2H_y$ alloys by microstructural manipulation. *Acta Materialia* 2021;207:116687. DOI
12. Wang Y, Zhang H, Liu E, et al. Outstanding comprehensive performance of $La(Fe, Si)_{13}H_y$/In composite with durable service life for magnetic refrigeration. *Adv Electron Mater* 2018;4:1700636. DOI
13. Fujita A, Fujieda S, Hasegawa Y, Fukamichi K. Itinerant-electron metamagnetic transition and large magnetocaloric effects in $La(Fe_xSi_{1-x})_{13}$ compounds and their hydrides. *Phys Rev B* 2003;67:104416. DOI
14. Jia L, Sun JR, Zhang HW, Hu FX, Dong C, Shen BG. Magnetovolume effect in intermetallics $LaFe_{13-x}Six$. *J Phys Condens Matter* 2006;18:9999-10007. DOI
15. Huang R, Liu Y, Fan W, et al. Giant negative thermal expansion in $NaZn_{13}$-type $La(Fe, Si, Co)_{13}$ compounds. *J Am Chem Soc* 2013;135:11469-72. DOI PubMed
16. Li W, Huang R, Wang W, et al. Enhanced negative thermal expansion in $La_{(1-x)}Pr_xFe_{10.7}Co_{0.8}Si_{1.5}$ compounds by doping the magnetic rare-earth element praseodymium. *Inorg Chem* 2014;53:5869-73. DOI PubMed
17. Li S, Huang R, Zhao Y, Wang W, Han Y, Li L. Zero thermal expansion achieved by an electrolytic hydriding method in $La(Fe,Si)_{13}$ compounds. *Adv Funct Mater* 2017;27:1604195. DOI
18. Li S, Huang R, Zhao Y, Wang W, Li L. Cryogenic abnormal thermal expansion properties of carbon-doped $La(Fe,Si)_{13}$ compounds. *Phys Chem Chem Phys* 2015;17:30999-1003. DOI PubMed
19. Li S, Huang R, Zhao Y, et al. Broad negative thermal expansion operation-temperature window achieved by adjusting Fe-Fe magnetic exchange coupling in $La(Fe,Si)_{13}$ compounds. *Inorg Chem* 2015;54:7868-72. DOI PubMed
20. Wang J, Gong Y, Liu J, et al. Balancing negative and positive thermal expansion effect in dual-phase $La(Fe,Si)_{13}$/α-Fe in-situ composite with improved compressive strength. *J Alloys Compd* 2018;769:233-8. DOI
21. Zhang H, Sun Y, Niu E, Hu F, Sun J, Shen B. Enhanced mechanical properties and large magnetocaloric effects in bonded $La(Fe, Si)_{13}$ -based magnetic refrigeration materials. *Appl Phys Lett* 2014;104:062407. DOI
22. Toby BH. EXPGUI, a graphical user interface for GSAS. *J Appl Crystallogr* 2001;34:210-3. DOI
23. Bird M, Butler S, Hawkes C, Kotzer T. Numerical modeling of fluid and electrical currents through geometries based on synchrotron X-ray tomographic images of reservoir rocks using Avizo and COMSOL. *Comput Geosci* 2014;73:6-16. DOI
24. Sun XM, Cong DY, Ren Y, et al. Giant negative thermal expansion in Fe-Mn-Ga magnetic shape memory alloys. *Appl Phys Lett* 2018;113:041903. DOI
25. Li S, Huang R, Li W, Wang W, Zhao Y, Li L. Low-temperature negative thermal expansion behavior of LaFe11.2Al1.8-xSix compounds. *J Alloys Compd* 2015;646:119-23. DOI
26. Lin JC, Tong P, Tong W, et al. Tunable negative thermal expansion related with the gradual evolution of antiferromagnetic ordering in antiperovskite manganese nitrides $Ag_{1-x}NMn_{3+x}$ ($0 \leq x \leq 0.6$). *Appl Phys Lett* 2015;106:082405. DOI
27. Xia W, Huang J, Sun N, Lui C, Ou Z, Song L. Influence of powder bonding on mechanical properties and magnetocaloric effects of

$La_{0.9}Ce_{0.1}(Fe,Mn)_{11.7}Si_{1.3}H_{1.8}$. *J Alloys Compd* 2015;635:124-8. DOI

28. Shao Y, Liu J, Zhang M, et al. High-performance solid-state cooling materials: Balancing magnetocaloric and non-magnetic properties in dual phase La-Fe-Si. *Acta Materialia* 2017;125:506-12. DOI
29. Wang W, Huang R, Dai H, et al. Tunable near-zero thermal expansion in the C-doped La(Fe, $Si)_{13}$ compounds at cryogenic temperatures. *Mater Lett* 2019;237:26-8. DOI
30. Hu J, Lin K, Cao Y, et al. Adjustable magnetic phase transition inducing unusual zero thermal expansion in cubic $RCO_2$-based intermetallic compounds (R = rare earth). *Inorg Chem* 2019;58:5401-5. DOI PubMed
31. Song Y, Chen J, Liu X, et al. Zero Thermal expansion in magnetic and metallic $Tb(Co,Fe)_2$ intermetallic compounds. *J Am Chem Soc* 2018;140:602-5. DOI PubMed
32. Fujita A, Fukamichi K, Yamada M, Goto T. Influence of pressure on itinerant electron metamagnetic transition in $La(Fe_xSi_{1-x})_{13}$ compounds. *J Appl Phys* 2003;93:7263-5. DOI
33. Lyubina J, Schäfer R, Martin N, Schultz L, Gutfleisch O. Novel design of $La(Fe,Si)_{13}$ alloys towards high magnetic refrigeration performance. *Adv Mater* 2010;22:3735-9. DOI PubMed